Identification of a chronic non-neurodegenerative microglia activation state in a mouse model of peroxisomal β-oxidation deficiency

Journal:	*GLIA*
Manuscript ID:	GLIA-00364-2014.R1
Wiley - Manuscript type:	Original Research Article
Date Submitted by the Author:	n/a
Complete List of Authors:	Verheijden, Simon; KU Leuven, Pharmaceutical and pharmacological sciences Beckers, Lien; KU Leuven, Pharmaceutical and pharmacological sciences Casazza, Andrea; KU Leuven, Vesalius Research Centre Butovsky, Oleg; Harvard Medical School, Neurology Mazzone, Massimiliano; VIB, Vesalius Research Centre Baes, Myriam; K.U.Leuven, Pharmaceutical Sciences
Key Words:	microglia, peroxisomes, mTOR, multifunctional protein 2

Identification of a chronic non-neurodegenerative microglia activation state in a mouse model of peroxisomal β-oxidation deficiency

Simon Verheijden[1]*, Lien Beckers[1]*, Andrea Casazza[2,3], Oleg Butovsky[4], Massimiliano Mazzone[2,3], Myriam Baes[1]

[1]KU Leuven - University of Leuven, Department of Pharmaceutical and Pharmacological Sciences, Cell Metabolism, B-3000 Leuven, Belgium; [2]KU Leuven - University of Leuven, Department of Oncology, Laboratory of Molecular Oncology and Angiogenesis, B-3000 Leuven, Belgium; [3]VIB, Vesalius Research Center, Laboratory of Molecular Oncology and Angiogenesis, B-3000 Leuven, Belgium; [4]Center for Neurologic Diseases, Department of Neurology, Brigham and Women's Hospital, Harvard Medical School, Boston, Massachusetts, USA

Running title: Microglia signature in peroxisomal MFP2 deficiency

Abstract: 230 words
Introduction: 854 words
Materials and methods: 1509 words
Results:1780 words
Discussion:1444 words
References:1948 words
Figure legends:1056 words
Number of figures: 6 + 1 supplemental figure
Number of tables:1 supplemental table

***: Equal contribution**

Corresponding author:
Myriam Baes, PhD
Laboratory for Cell Metabolism
Faculty of Pharmaceutical and Pharmacological Sciences
Campus Gasthuisberg O/N2
Herestraat 49
B 3000 Leuven
Tel + 32 16 330853
Fax + 32 16 330856
e-mail: Myriam.Baes@pharm.kuleuven.be

MAIN POINTS:

- Resident microglia in MFP2 deficient mice exhibit a proliferative and immunologically activated state but they lack signs of phagocytic and neurotoxic activity
- The chronically reactive microglia lose their typical homeostatic markers but upregulate pathways associated with growth and proliferation
- The molecular signature of microglia in *Mfp2*$^{-/-}$ brain strongly diverges from microglia in the neurodegenerative milieu of an ALS mouse model

KEYWORDS
Neuroinflammation, microglia, peroxisomes, phagocytosis

ABSTRACT

The functional diversity and molecular adaptations of reactive microglia in the chronically inflamed central nervous system (CNS) are poorly understood. We previously showed that mice lacking multifunctional protein 2 (MFP2), a pivotal enzyme in peroxisomal β-oxidation, persistently accumulate reactive myeloid cells in the gray matter of the CNS. Here we show that the increased numbers of myeloid cells solely derive from proliferation of resident microglia and not from infiltrating monocytes. We defined the signature of *Mfp2*$^{-/-}$ microglia by gene expression profiling after acute isolation, which was validated by quantitative PCR, immunohistochemical and flow cytometric analysis. The features of *Mfp2*$^{-/-}$ microglia were compared with those from SOD1^{G93A} mice, an amyotrophic lateral sclerosis model. In contrast to the neurodegenerative milieu of SOD1^{G93A} spinal cord, neurons were intact in *Mfp2*$^{-/-}$ brain and *Mfp2*$^{-/-}$ microglia lacked signs of phagocytic and neurotoxic activity. The chronically reactive state of *Mfp2*$^{-/-}$ microglia was accompanied by downregulation of markers that specify the unique microglial signature in homeostatic conditions. In contrast, mammalian target of rapamycin (mTOR) and downstream glycolytic and protein translation pathways were induced, indicative of metabolic adaptations. *Mfp2*$^{-/-}$ microglia were immunologically activated but not polarized to a pro- or anti-inflammatory phenotype. A peripheral lipopolysaccharide challenge provoked an exaggerated inflammatory response in *Mfp2*$^{-/-}$ brain, consistent with a primed state. Taken together, we demonstrate that chronic activation of resident microglia does not necessarily lead to phagocytosis nor overt neurotoxicity.

INTRODUCTION

Microglia, the resident immune cells of the CNS, are actively engaged in both homeostasis and pathology in the adult brain. Under physiological conditions, microglia constantly survey the microenvironment and communicate in a bidirectional way with neural cells (Ransohoff and Perry, 2009, Hughes, 2012, Gomez-Nicola et al., 2013, Prinz and Priller, 2014). It has become clear that microglia play a critical role in neuronal plasticity by controlling synaptic function and synaptogenesis (Tremblay et al., 2010, Salter and Beggs, 2014). Recently, important progress was made in the molecular characterization of homeostatic microglia, by differentiating their transcriptome signature from that of neural cells and other myeloid cells (Butovsky et al., 2012, Gautier et al., 2012, Chiu et al., 2013, Hickman et al., 2013, Butovsky et al., 2014).

In addition to their role in CNS homeostasis, microglia sense CNS damage and can act as versatile effector cells during neuropathological conditions. To this end, microglia adopt a range of activation states which remain ill-defined at the molecular level. In particular, the diverse phenotypes of microglia in conditions of chronic stress in the brain are poorly understood (Gomez-Nicola et al., 2013, Cherry et al., 2014). The morphological transition from ramified to amoeboid is accompanied by new effector functions that can vary widely and encompass proliferation, migration, production of cytokines and chemokines, and phagocytic activity. Whether chronically activated microglia always attain neurotoxic properties is still a matter of debate (Biber et al., 2014). An undervalued aspect in chronic neuroinflammation is that concomitant with acquiring novel shapes and functions, microglia might also lose features related to their homeostatic role. To better understand the spectrum of phenotypes of reactive microglia, information on gene expression and insights in signaling pathways are necessary. Recently, the microglia transcriptome of $SOD1^{G93A}$ mice, an amyotrophic lateral sclerosis (ALS) model was defined (Butovsky et al., 2012, Chiu et al., 2013). These microglia concurrently upregulate both neurotoxic and neuroprotective factors as well as genes associated with lysosomal activity and phagocytosis (Chiu et al., 2013). Their molecular profile was different from that of lipopolysaccharide (LPS)-activated microglia and of M1 or M2 macrophages, and was denoted as a neurodegeneration-specific signature (Chiu et al., 2013).

Chronic microglia activation is an important hallmark of many neurodegenerative diseases and contributes significantly to the progression of these disorders (Glass et al., 2010). Moreover, microglial

dysfunction might underlie some neurological disorders, such as Rett's syndrome (Derecki et al., 2013) and Nasu-Hakola disease (Satoh et al., 2011). Also in X-linked adrenoleukodystrophy, a neurometabolic disorder caused by peroxisomal β-oxidation deficiency (Kemp et al., 2012), microglia seem to play a pivotal role in disease pathogenesis. This is inferred from the therapeutic efficacy of bone marrow transplantation or hematopoietic stem cell gene therapy to halt the inflammatory demyelination seen in the cerebral childhood form of the disease (ccALD) (Cartier et al., 2009, Cartier and Aubourg, 2010). Due to the absence of neuroinflammation in the corresponding mouse model (*Abcd1*$^{-/-}$), the precise molecular abnormalities leading to cerebral inflammation and/or microglial dysfunction cannot be investigated (Kemp et al., 2012). Interestingly, we recently showed that mice lacking multifunctional protein-2 (MFP2; also known as D-bifunctional protein), a peroxisomal β-oxidation enzyme downstream of the ABCD1 transporter, develop robust neuroinflammation (Huyghe et al., 2006c, Verheijden et al., 2013). This initiates before the age of 8 weeks and is confined to the gray matter throughout the brain and spinal cord. The expanding inflammation parallels the aggravating neurological phenotype of the mice, characterized by motor and cognitive impairments, lethargy and death before the age of 6 months ((Huyghe et al., 2006c) and unpublished observations). With the exception of testicular degeneration, no peripheral organ failure was observed (Jia et al., 2003, Huyghe et al., 2006a, Huyghe et al., 2006b). Interestingly, mice with selective elimination of MFP2 from neural cells develop minor neuroinflammation and have an extended lifespan compared to general knockouts (Verheijden et al., 2013). This suggests that loss of peroxisomal β-oxidation from non-neural cells (e.g. microglia and/or infiltrating monocytes) worsens the inflammatory state of the brain.

For unknown reasons, the phenotype of *Mfp2*$^{-/-}$ mice deviates from the severe neurodevelopmental pathology of patients with total ablation of MFP2 (Ferdinandusse et al., 2006b). Milder mutations give rise to degenerative neurological anomalies including ataxia, leukodystrophy and vision/hearing problems (Ferdinandusse et al., 2006a, Khan et al., 2010, van der Knaap et al., 2012) but it has not been assessed whether neuroinflammation develops. The precise metabolic role of MFP2 in the formation and maintenance of the CNS remains unresolved. Apart from increased levels of very long chain fatty acids, no other metabolic anomalies have been identified (Huyghe et al., 2006a).

In this study, we used *Mfp2*$^{-/-}$ mice as a unique tool to study the cellular and molecular aspects of neuroinflammation in peroxisomal β-oxidation deficiency. Specifically, we aimed to molecularly define the activation state of microglia and to uncover the cellular mechanisms driving the neuroinflammatory response. Our findings show that *Mfp2*$^{-/-}$ microglia adopt a strongly proliferative and immunologically activated phenotype that is neuron-sparing. As this contrasts with microglia in the neurodegenerative milieu of the *SOD1*^{G93A} spinal cord (Chiu et al., 2013), we directly compared gene expression and histological features of microglia in both mouse models.

MATERIALS AND METHODS

Mouse breeding

The generation of *Mfp2*$^{-/-}$ mice has been described (Baes et al., 2000). *Mfp2*$^{-/-}$ mice were bred on a Swiss/Webster background in the specific pathogen free animal housing facility of the KU Leuven, had *ad libitum* access to water and standard rodent food, and were kept on a 12-hour light and dark cycle. As we did not detect differences between wild type and heterozygous mice in our previous investigations, they were both used as controls. Unless stated otherwise, all experiments were performed on 17-20 week old mice with mixed gender and were in accordance with the "Guidelines for Care and Use of Experimental Animals" and fully approved by the Research Ethical committee of the KU Leuven (#190/2012).

Microglia isolation by FACS sorting

Microglia were acutely isolated from *Mfp2*$^{-/-}$ and control mice (n=4 for each genotype). After transcardiac perfusion with ice-cold PBS, brains were quickly dissected and mechanically homogenized with a tissue homogenizer in ice-cold HBSS containing 15mM HEPES and 0.5 % glucose (De Haas et al., 2007). Cells were filtered over a 70 µm strainer and pelleted at 220 g for 10 min at 4 °C. Contaminating myelin was removed by resuspending the pellet in 25 ml ice-cold 22% Percoll buffer, overlaying with 5 mL ice-cold PBS followed by centrifugation in a swinging bucket rotor at 950 g for 25 min at 4 °C (modified from (Olah et al., 2012)). The cells were incubated with mouse anti-CD45-FITC (eBiosciences 11-0451; 1:40) and mouse anti-CD11b-APC (eBiosciences 17-0112; 1:100) for 30 minutes at 4 °C in the dark. CD11b^{high}/CD45^{mid} cells were isolated using an Aria I fluorescence-activated cell sorter (FACS) (BD Biosciences) equipped with a 488 nm and 633 nm

laser. Cells with low forward/sideward scatter profile were excluded from the isolation. Microglia yield ranged between 1 x 10^5 to 3 x 10^5 cells/mouse brain. Cells were collected in RNA lysis buffer provided with the RNeasy microkit (Qiagen, 74004). Data from FACS sorting of $CD11b^{high}/CD45^{mid}$ myeloid cells were analyzed using BD FACsuite software (BD Biosciences).

Microarray

Total RNA was isolated from FACS sorted microglia by using the RNeasy Micro kit (Qiagen). The quality of the RNA samples was determined with an Agilent 2100 Bioanalyzer (Agilent Technologies, California, USA). Only samples with RIN values (RNA Integrity Number) higher or equal to 8 were used. The RNA was amplified with the NuGEN amplification kit (Agilent technologies). For microarray analysis, the whole genome GeneChip Mouse Gene 1.0 ST Array was used as described previously. Quality control, amplification, labeling of the samples, hybridization, washing and scanning of the chips and first-line bioinformatics was carried out at the MicroArray Facility (MAF, VIB, Leuven, Belgium). The complete dataset is available under GEO record GSE66420.

Flow cytometry

Brain cells were isolated by Percoll gradient centrifugation as described above. For antibody labeling, 1 x 10^5 cells were incubated in 200 µl for 20 min at 4 °C with combinations of mouse anti-Cd11b-APC (1:200) and either rat anti-LY6C-FITC (1:200), rat anti-5E12 (CD39) (1:300) rat anti-FCRLS (1:300) antibodies (Butovsky et al., 2012, Butovsky et al., 2014). The latter two were detected with goat anti-rat IgG conjugated to FITC (1:300; BioLegend). To demonstrate cell proliferation, bromodeoxyuridine (BrdU) (Sigma B5002) was dissolved in sterile Dulbecco's phosphate buffered saline at 37°C and injected intraperitoneally (50 mg/kg body weight) daily for 3 consecutive days in 12-week-old or 16-week-old *Mfp2* knockout and wild type littermates. Twelve hours after the last BrdU injection, proliferating cells were detected using flow cytometry with anti-BrDU antibodies (BrDU Flow Kit; BD Biosciences). Alternatively, animals were sacrificed for immunohistochemical detection of BrdU. Flow cytometry was performed on a FACSVerse (BD Biosciences), and data analyzed with BD FACsuite software (BD Biosciences). For immunological profiling, CD11b-Pe Cy7 (clone M1/70, Biolegend) was used in combination with CD11c-APC (clone HL3, BD Pharmingen), F4/80-APC (clone BM8, eBioscience), CX3CR1-FITC (Goat polyclonal, R&D Systems), CD204-Alexa 647 (clone MR5D3, AbD

Serotec), CD206-Alexa 647 (clone 2F8, AbD Serotec) or IL10R (Imtec Diagnostics) all at dilutions of 1:200.

Real time PCR

Real time PCR was performed as previously described (Bottelbergs et al., 2010) using an ABI PRISM 7500 Real Time PCR instrument (Applied Biosystems, Lennik, Belgium). Primers and probes were either designed using Primer Express Software (Applied Biosystems) (β-actin, iNOS, Tnf sequences available on request) or ordered from Applied Biosystems as premade Taqman Gene Expression assays (Il1b, Mm011336189_m1; Il6, Mm01210733_m1; Cx3cr1, Mm0262011_s1; Tgfbr1, Mm00436964_m1; arginase, Mm00475991_m1; Mrc1, Mm00485148_m1). Assays were performed in duplicate or triplicate in 10 µL TaqMan Fast Universal PCR Master Mix (Applied Biosystems). Relative expression levels of the target genes were calculated taking into account the amplification efficiency as described (Giulietti et al., 2001). The relative expression levels of the target genes were calculated as a ratio to the housekeeping gene β-actin.

Bioinformatics

Differential expression of genes between the two conditions is based on the robust multi-array analysis (RMA) expression values (Irizarry et al., 2003) as obtained with the xps package (version 1.18.1) of BioConductor (www.bioconductor.org). We tested whether it significantly deviates from 0 with a moderated t-statistic (implemented in limma). The resulting p-values are corrected for multiple testing with Benjamini-Hochberg (Hochberg and Benjamini, 1990) to control the false discovery rate. In general, differential expression is based on the p-values, corrected for multiple testing (e.g. all probes with a corrected p-value less than 0.01) together with a cut-off on the fold-change of 1.5. Pathway analysis is based on information provided by The Ingenuity Knowledge Base. For data interpretation and visualization Ingenuity pathway analysis (IPA) and the functional annotation tool KEGG (Kyoto Encyclopedia for Genes and Genomes database) from DAVID (Database for Annotation, Visualization and Integrated Discovery v6.7) was used. In addition, the dataset from *Mfp2*$^{-/-}$ microglia was compared to transcriptomics datasets based on either RNA-sequencing of microglia in homeostatic conditions and from SOD1^{G93A} mice (Chiu et al., 2013) (GEO dataset GSE43366) or gene expression profiling of microglia in homeostatic conditions using a NanoString nCounter platform

(Butovsky et al., 2014). The RPKM gene levels from the RNA-seq experiment were converted to fold change as compared to control values. Differentially expressed genes (fold > 1.5, p-value < 0.01) were used for all analyses.

Histology

Anesthesia of the mice and tissue processing and immunohistochemical (IHC) staining were performed as described (Hulshagen et al., 2008). Routinely, paraffin sections (7 µm) were used for immunofluorescent stainings. The following primary antibodies were used: polyclonal rabbit anti-Iba1 (1:500; Wako D19-19741), rabbit anti-phospho-S6 ribosomal protein mAb (Ser235/236) (1:400; Cell signaling D57.2.2E), rabbit Cathepsin D (1:200 Santa Cruz), Lamp2/Mac3 (1:100, BD Pharmingen), rat Anti-BrDU mAb (1:100; AbD Serotec OBT0030), rabbit 3-nitrotyrosine (1:100; Millipore 06-284), and rabbit 4-hydroxynonenal (1:500; Millipore 393204). Cryo sections were used for staining with polyclonal rabbit anti-P2RY12 (1:500; provided by Prof. O. Butovsky, Boston, USA). Frozen sections of spinal cord of endstage $SOD1^{G93A}$ mice were kindly provided by Prof. L. Van Den Bosch (VIB and KU Leuven, Belgium). After incubation with primary antibodies overnight at room temperature (at 4°C for anti-P2RY12 staining) HRP-labeled secondary antibodies (1:200) were applied for 1 hour, followed by fluorescent labeling with a cyanine 2 (FITC) TSA kit (Perkin Elmer Life sciences, Boston, USA). P2ry12 antibodies were detected with goat anti-rabbit IgG conjugated to Alexa647 (1:300; Life technologies A21244). When double immunolabeling was performed, sets of primary and secondary antibodies were applied sequentially. As second fluorescent labels, cyanine 3 TSA kits (Perkin-Elmer) were used. Images were acquired with a motorized inverted IX-81 microscope connected to a CCD-FV2T digital camera (Olympus, Aartselaar, Belgium) and processed with LSM Image browser software (Zeiss, Germany). Microglia cell numbers were quantified on Iba-1 immunofluorescent stained paraffin sections (7 µm) around the sagittal midline (n=4). Within one plane (20 x magnification), only Iba-1-positive cells that fully colocalized with DAPI-positive nuclei were counted in the different regions of the brain, namely cornu ammonis (CA) 1-3 and dentate gyrus (DG) of hippocampus, somatosensory cortex, motor cortex and dorsal pons. Microglia number/frame was corrected for surface area. Quantification of neuronal numbers in CA3 of hippocampus was performed on cresyl violet stained sections (n=5) in a similar way as described for microglia. Only cells in which the Nissl substance was clearly visible were quantified. .

In vivo LPS challenge and cytokine measurements

Mfp2$^{-/-}$ and control mice 14 weeks of age received an intraperitoneal injection of LPS (1mg/kg, Sigma, L4391) or sterile saline vehicle in a total volume of 100µl. Four hours later, mice were sacrificed, plasma and brain regions were collected and flash frozen in liquid nitrogen. Brainstem was homogenized 1:10 (w/v) in ice-cold PBS containing a cocktail of protease inhibitors (Roche) and lysates were cleared by centrifugation at 14000g for 20 min at 4°C. Immunoreactive levels of TNF, IL1β and IL6 were measured in plasma and brainstem lysates by using a cytometric bead array mouse soluble protein flex set system (BD Biosciences). The samples were prepared according to the manufacturer's instructions and analyzed on a FACSCanto HTS (BD Biosciences) and analyzed by FCAP array software (BD Biosciences).

Statistical analysis

One-way ANOVA was carried out using Graphpad Prism 3.0 software (San Diego, CA). For microarray data, p-values are corrected for multiple testing with Benjamini-Hochberg (Hochberg and Benjamini, 1990).

RESULTS

No invasion of Ly6C$^+$ monocytes but proliferation of resident microglia in *Mfp2*$^{-/-}$ brain

One of the most striking neuropathological hallmarks of *Mfp2*$^{-/-}$ mice is the development of extensive neuroinflammation involving astro- and microgliosis (Huyghe et al., 2006c, Verheijden et al., 2013). During the disease course, Iba1$^+$ brain macrophages acquire an activated phenotype and display enlarged cell bodies and a deramified morphology together with increased F4/80 expression (Verheijden et al., 2013). In order to estimate whether these cells increase in number, Iba1$^+$ cells were quantified in different regions of the CNS of mice at end stage (5 months old). In hippocampus, motor cortex and pons, microglia/macrophage numbers were 4-6 fold increased in *Mfp2*$^{-/-}$ compared to control brain (Fig. 1A). To investigate whether this increase arises from influx of peripheral monocytes or accumulation of resident microglia, we evaluated the presence of markers that are respectively expressed by blood monocytes (Ly6C) and resident microglia (CD39, FCRLS). Indeed, *Butovsky et al* recently showed that the expression of Ly6C and CD39/FCRLS effectively distinguishes non-overlapping populations of peripheral inflammatory monocytes and CNS-resident microglia in mice (Butovsky et al, 2012; Butovsky et al, 2014). The efficacy of these discriminating markers has been convincingly proven in a mouse model of ALS (SOD1^{G93A})(Butovsky et al., 2012, Butovsky et al., 2014). FACS analysis on brain homogenates of endstage *Mfp2*$^{-/-}$ mice showed that almost all CD11b$^+$ cells are negative for the monocyte marker Ly6C (> 99%) (Fig.1B). In contrast, the vast majority of CD11b$^+$ cells (> 97%) is positive for CD39 and FCRLS, two specific markers for resident microglia (Fig. 1C-D). Moreover, all CD11b$^+$ cells are CD45^{dim}, which is another characteristic of resident microglia (data not shown). Together, these data show that the expanded myeloid population is of local origin allowing to further designate these cells as microglia.

Having excluded influx of inflammatory monocytes in the *Mfp2*$^{-/-}$ brain, we next wanted to verify whether the accumulation of brain myeloid cells originates from proliferation of CNS resident microglia. We analyzed BrdU incorporation in microglial cells and indeed found significantly increased numbers of proliferating Iba1$^+$/BrdU$^+$ cells by IHC analysis (Fig. 1E) and Cd11b$^+$/BrdU$^+$ cells by FACS analysis in *Mfp2*$^{-/-}$ compared to control mice (Fig. 1F,G). Together, these data demonstrate that the inflammatory response in *Mfp2*$^{-/-}$ brain is governed by proliferation of resident microglia and not by infiltration of peripheral cells.

Defining the molecular signature of a non-neurodegenerative microglia phenotype

As microgliosis in *Mfp2*$^{-/-}$ mice is confined to gray matter areas such as cortex, hippocampus and brainstem (Verheijden et al., 2013), we performed double immunofluorescence stainings with microglial and neuronal markers. We observed that microglia enwrap neuronal cell bodies (Fig. 2A-F), suggesting that microglia in *Mfp2*$^{-/-}$ mice become activated in response to neuronal demise, analogous to several disease models of neurodegenerative disorders. However, previous FluoJade and caspase/TUNEL stainings did not show evidence for neuronal damage nor death in the CNS of *Mfp2*$^{-/-}$ mice (Huyghe et al., 2006c). To further confirm the conservation of neurons, we counted neuron numbers in the CA3 region of the hippocampus of endstage *Mfp2*$^{-/-}$ mice (Fig. 2G-I). We did not find significant differences between *Mfp2*$^{-/-}$ and control mice. Also in other brain regions, we could not detect an overt reduction of neuron numbers (not shown). The microglia microenvironment in *Mfp2*$^{-/-}$ brain thus deviates from the milieu in neurodegenerative disorders. We therefore characterized the molecular signature of this non-neurodegenerative microglia phenotype and performed microarray analysis on acutely isolated microglia (CD11b^{+}/CD45^{dim}) from whole brain of 5 months old control and *Mfp2*$^{-/-}$ mice (Fig. 3A,B). We found that 983 genes were differentially expressed in *Mfp2*$^{-/-}$ compared to control microglia (288 downregulated, 695 upregulated; fold ≥ 1.5, p-value < 0.01) (Fig. 3C). The top 50 up- and downregulated genes, the unsupervised hierarchical clustering of RMA values and the principle component analysis of gene expression data are shown in Suppl. Fig.1. Pathway enrichment by Ingenuity and DAVID analysis demonstrated pronounced induction of pathways related to protein translation, cellular growth and proliferation, such as *Eif2 signaling*, *mTOR signaling* and *regulation of eIF4 and p70S6K signaling* (Fig. 3D and Suppl. Table 1). Activation of mTOR was validated by IHC, showing increased phosphorylation of the downstream target ribosomal S6 protein (pS6) in *Mfp2*$^{-/-}$ compared to wild type microglia (Fig. 3E,F). The transcription factor Hypoxia-inducible factor 1-alpha (HIF1α), another downstream target of mTOR (Duvel et al., 2010), was significantly induced according to the microarray data, which was further supported by elevated transcripts of several enzymes of the glycolytic pathway and VEGF (Suppl. Table 1). Interestingly, the regulatory subunit of 5' AMP-activated protein kinase (AMPK) that inhibits mTOR in conditions of cellular energy depletion, was downregulated by 50%. The enrichment of mTOR and eIF2 signaling is in accordance with the strong proliferative response and cellular growth observed in *Mfp2*$^{-/-}$ microglia.

Microglia in *Mfp2*$^{-/-}$ brain are not phagocytic and do not produce reactive oxygen/nitrogen species

We compared the transcriptional signature of *Mfp2*$^{-/-}$ microglia residing in a neuron-sparing milieu, with the previously published neurodegeneration-specific microglial signature in *SOD1*^{G93A} mice, a model for ALS (GEO dataset GSE43366)(Chiu et al., 2013). The most pronounced difference between the *Mfp2*$^{-/-}$ and *SOD1*^{G93A} model was the strong enrichment of the KEGG pathway *Lysosome* in *SOD1*^{G93A} microglia (37.9% of genes related to *Lysosome* upregulated) (Fig. 4B) whereas this was less obvious for *Mfp2*$^{-/-}$ microglia (11.7% of genes upregulated) (Fig. 4A). Comparison for enriched functions between the two models using Ingenuity analysis demonstrated marked enrichment for 'phagocytosis', 'cytoskeletal organization' and 'respiratory burst' in the *SOD1*^{G93A} as compared to *Mfp2*$^{-/-}$ microglia (Fig. 4C). As these data suggest that microglia in *Mfp2*$^{-/-}$ mice do not acquire phagocytic properties, in contrast to microglia in a neurodegenerative disease model (*SOD1*^{G93A}), we performed IHC for markers associated with lysosomal activation and phagocytosis. There was no increased immunoreactivity of Cathepsin D (Fig. 4D,E), LAMP2/MAC3 (Fig. 4G,H) and CD68 (not shown) in brain of *Mfp2*$^{-/-}$ versus control mice (shown for visual cortex and brainstem). In contrast, we detected clear positive staining for these markers in the lumbal spinal cord of endstage *SOD1*^{G93A} mice (Fig. 4F,I).

The low expression of 'respiratory burst' genes in *Mfp2*$^{-/-}$ as compared to *SOD1*^{G93A} microglia comprised normal levels of *Nos2*, *Nox1* and *Nox2* (*Cybb*) versus controls. In contrast, *SOD1*^{G93A} microglia showed a very strong upregulation of *Cybb* compared to control microglia (> 40 fold) (Chiu et al., 2013). As reactive oxygen and nitrogen species are known to be important mediators of neurotoxicity, and upregulation might take place at the posttranscriptional level, we further evaluated oxidative stress markers. IHC stainings for nitrated proteins (Fig. 4J-L) and lipid peroxidation (4HNE, not shown) were not detectable in *Mfp2*$^{-/-}$ brain (Fig. 4K), whereas both were positive in *SOD1*^{G93A} spinal cord (Fig. 4L and data not shown).

In summary, despite their chronic active state, *Mfp2*$^{-/-}$ microglia do not upregulate pathways associated with phagocytic clearance, lysosomal activity and reactive oxygen/nitrogen species production. This is in striking contrast to the neurodegeneration-specific microglial signature of *SOD1*^{G93A} mice.

367 **_Mfp2_$^{-/-}$ microglia are immunologically activated but not polarized**

368 In response to disruption of CNS homeostasis by infectious or sterile conditions, reactive microglia can
369 produce pro-inflammatory cytokines such as TNF. Chronic release of these substances by microglia
370 can affect neuronal viability (Block et al., 2007). In contrast, the induction of an anti-inflammatory
371 microglia phenotype is generally linked to neuroprotection (Kigerl et al., 2009, Liao et al., 2012). In
372 view of preserved neuron numbers in *Mfp2*$^{-/-}$ mice and the absence of a neurodegeneration-specific
373 microglial signature, we explored transcript levels of genes associated with pro- and anti-inflammatory
374 activation in the micro-array dataset. Microglia in *Mfp2*$^{-/-}$ mice are clearly immunologically activated as
375 several genes encoding cytokines (*Il1b, Tnf, Il12b*), chemokines (*Ccl5, Ccl2*) and surface markers
376 (*Itgax, Emr1, Cd83, Cd86*) associated with inflammatory activation were strongly induced (Fig. 5A,C).
377 Remarkably, the expression of several key pro-inflammatory genes was unchanged (*Nos2, Il12a,*
378 *Cxcl9, Ifnb1, Icam1*) or even downregulated (*Il6*), suggesting that microglia in *Mfp2*$^{-/-}$ mice do not
379 acquire a typical pro-inflammatory activation state. However, *Mfp2*$^{-/-}$ microglia could also not be
380 categorized as anti-inflammatory, because typical anti-inflammatory genes were either induced (*Arg1,*
381 *Msr1*) or repressed (*Mrc1, Stab1*) (Fig. 5A-C). qRT-PCR and FACS analysis of some key inflammatory
382 markers further confirmed that the microglia activation state in *Mfp2*$^{-/-}$ mice cannot be categorized as
383 pro- or anti-inflammatory (Fig. 5B,D). Analysis of cytokine levels in brain homogenates revealed that
384 despite strongly increased transcript levels of *Tnf* and *Il1b* in microglia, the respective cytokine levels
385 were not detectable (TNF) or only 1.5 fold increased (IL1β) (not shown) in *Mfp2*$^{-/-}$ brain, further
386 supporting the absence of a typical pro-inflammatory effector state. Interestingly, after intraperitoneal
387 injection of LPS, both transcript (Tnf, Il1b) and protein levels (IL1β, IL6 and TNFα) were more strongly
388 induced in *Mfp2*$^{-/-}$ compared to control mice, consistent with a primed state (Perry and Holmes, 2014)
389 (Fig. 5E,F). In order to exclude that this particular immunological state of microglia is induced by
390 systemic inflammation, we analyzed cytokine levels in plasma (Il1β, Il6, TNFα) and the leucocyte
391 profile in blood. There were however no signs of peripheral inflammatory anomalies in *Mfp2*$^{-/-}$ mice
392 and after LPS administration cytokine levels increased similarly in control and mutant mice (data not
393 shown).
394 It thus seems that *Mfp2*$^{-/-}$ microglia exhibit an immunologically activated and primed state, but they are
395 not polarized and only acquire a typical pro-inflammatory effector state after a secondary stimulus.
396

The homeostatic microglial signature is downregulated in *Mfp2*$^{-/-}$ microglia

Several research groups recently reported the specific transcript signature of homeostatic microglia (Gautier et al., 2012, Chiu et al., 2013, Hickman et al., 2013, Butovsky et al., 2014) by comparing the transcriptomes of microglia with those of other CNS cell types and/or peripheral myeloid cells. This resulted in the identification of specific markers of microglia in their surveillance mode. When comparing our data set with the homeostatic microglial signature, it was conspicuous that the bulk of microglia specific genes was significantly suppressed in *Mfp2*$^{-/-}$ microglia (46% when compared with Butovsky et al.(Butovsky et al., 2014) (Fig. 6A) and 53 % compared with Chiu et al. (Chiu et al., 2013)), whereas only a few were upregulated (6-9%). These data demonstrate that in the inflamed *Mfp2*$^{-/-}$ brain, microglia loose typical features related to their homeostatic function. In order to validate the microarray data, we performed qRT-PCR of *Cx3cr1* and *Tgfbr1* on isolated microglia (Fig. 6B,C) and IHC analysis of P2RY12 (Fig. 6D,E) which confirmed the downregulation of these surface markers in *Mfp2*$^{-/-}$ microglia. FACS analysis for CX3CR1 and IL10R showed a clear reduction in CX3CR1 expression and a slight reduction in IL10R expression (Fig. 6F,G). Taken together, a hallmark of the microglia phenotype in *Mfp2*$^{-/-}$ brain is the loss of surface and other markers that were shown to be highly and exclusively expressed in these cells in homeostatic conditions.

DISCUSSION

This study contributes to a better understanding of the wide spectrum of phenotypes that microglia can adopt in the diseased brain. We determined the microglial signature in a murine model of peroxisomal β-oxidation deficiency in which robust and chronic inflammation in the gray matter occurs in the absence of neuronal loss. We show that the resident microglia in *Mfp2*$^{-/-}$ mice proliferate, are permanently in an activated non-phagocytic state and lose their typical homeostatic markers. Our data prove that microglia can remain in a reactive state without acquiring overt neurotoxic and phagocytic properties.

As infiltrating bone marrow-derived monocytes may have a major impact on the pathological course of neurological conditions (Prinz and Mildner, 2011, Yamasaki et al., 2014), it was of prime importance to establish the source of the expanded microglial compartment in *Mfp2*$^{-/-}$ mice. Analysis of specific markers corresponding to peripheral monocytes and resident microglia clearly showed that the myeloid cells in *Mfp2*$^{-/-}$ brain, even at late stages of disease, solely derive from local microglia. This differs from the neuroinflammatory demyelination condition in the peroxisomal β-oxidation disorder, ccALD in which the fast progressive phase coincides with opening of the blood brain barrier (Kemp et al., 2012).

Although the immunological profile of *Mfp2*$^{-/-}$ microglia is clearly distinct from naive microglia, the affected cytokines and inflammatory mediators could not be clustered in currently known pro- or anti-inflammatory states. In contrast to acute insults to the brain, where microglia switch from an initial pro-inflammatory to a resolving anti-inflammatory state, the microglial phenotype in chronic sterile stress conditions can be very heterogeneous. In the *SOD1*^{G93A} mouse model of ALS, microglia were shown to convert during the course of disease from an alternatively activated to a classically activated state (Liao et al., 2012). The latter were shown to be neurotoxic to motor neurons in vitro. It is now recognized that microglia induce inflammatory markers in the aged rodent brain and it is hypothesized that this modest chronic neuroinflammation impairs neuronal functioning (Norden and Godbout, 2013). Age is not contributing to the inflammatory response in our model as mice only survive up to 5-6 months of age. It remains however unsolved whether long-term activation of microglia is necessarily deleterious for neural cells (Biber et al., 2014). Interestingly, crucial players in the neurotoxic

properties are reactive oxygen and nitrogen species (Block et al., 2007, Brown and Neher, 2014). Although a set of pro-inflammatory surface and cytokine markers are induced in *Mfp2*$^{-/-}$ microglia, the genes responsible for generation of reactive oxygen and nitrogen species are not upregulated, even at endstage of disease. The induction of *Arg1*, a well characterized anti-inflammatory marker gene, also indicates that *Mfp2*$^{-/-}$ microglia are rather protective for their environment than toxic. Indeed, the enzyme arginase 1 utilizes, similar to iNOS, arginine as a substrate, but converts it to products that serve as precursors in repair processes and not to destructive nitrogen species (Lange et al., 2004, Estevez et al., 2006).

Gene expression screening and histological analyses further indicated absence of lysosomal activity and cytoskeletal remodeling that normally accompany phagocytosis. This is in sharp contrast with the gene expression signature of *SOD1*^{G93A} microglia in which these pathways were strongly induced (Chiu et al., 2013). In the latter model, microglia respond to early changes in motor neurons and develop phagocytic and neurotoxic properties even in a presymptomatic stage (Sanagi et al., 2010). On the contrary, reactive microglia in *Mfp2*$^{-/-}$ brain seem to get stuck in their graded response from a ramified to a fully activated phagocytic state. This raises the question whether *Mfp2*$^{-/-}$ microglia have the ability to develop lysosomal activity and execute phagocytosis. In this respect it is important to note that cathepsin D positive microglia were present in cerebellar white matter (data not shown), where we previously showed degeneration of Purkinje cell axons (Verheijden et al., 2013), indicative of a proper phagocytic function. Microglia in MFP2 deficient mice thus transform for a prolonged period in a reactive state that lacks neurodestructive behavior within their lifetime. It needs to be elucidated whether this state is triggered by cell autonomous processes in microglia resulting from peroxisomal β-oxidation inactivity or by microglial responses to MFP2 deficiency in neighbouring cells or a combination of these mechanisms. The fact that the microglial reactivity is confined to the gray matter strongly suggests that metabolic distress caused by peroxisomal MFP2 deficiency in neurons contributes to pathology.

In view of the seemingly harmless microglial activation, the question arises whether this contributes to disease pathogenesis in *Mfp2*$^{-/-}$ mice as increasing microgliosis coincides with the neurological symptoms. In this respect, it should be emphasized that the most prominent coordinated change in *Mfp2*$^{-/-}$ microglia is rather a loss-of-function than a toxic-gain-of-function. Several research groups

recently defined the unique transcriptome signature of homeostatic microglia by comparison with their neural cell neighbors and myeloid cell family members (Gautier et al., 2012, Chiu et al., 2013, Hickman et al., 2013, Butovsky et al., 2014). These typical microglial markers were generally downregulated in *Mfp2*$^{-/-}$ microglia pointing to a loss of their surveillance state. Butovsky et al recently reported that the microglia specific gene signature is mainly driven by transforming growth factor β (TGFβ) and that loss of TGFβ signaling leads to downregulation of the homeostatic gene signature (Butovsky et al., 2014). In *Mfp2*$^{-/-}$ microglia the expression of *Tgbr1* was downregulated, probably contributing to their loss-of-homeostatic-function phenotype. A large fraction of the downregulated genes encode cell surface proteins such as the purinergic receptors P2RY12 and P2RY13. It should however be noted that this loss of microglial membrane proteins is selective as several others are either unchanged (e.g. P2RY6) or increased (e.g. P2RX4) in expression. It is plausible that these alterations will perturb the microglial communication with the microenvironment or that chronic deprivation of homeostatic microglial properties impairs neurological function. It was indeed shown that lack of CX3CR1 signaling in microglia perturbs synaptic function in the postnatal period resulting in persistently disturbed brain connectivity and behavioral disorders (Zhan et al., 2014). Furthermore, loss of microglia in adulthood was proven to impact on memory and motor learning through impaired synapse formation, emphasizing the importance of proper neuron-microglia crosstalk in normal brain functioning (Parkhurst et al., 2013).

Whereas the primary trigger for microglia activation in *Mfp2*$^{-/-}$ brain remains unknown, we found that mTOR and other pathways driving protein synthesis were induced in the reactive microglia. Activation of these pathways leads to cell proliferation and growth, in line with the observed morphological and mitogenic response of *Mfp2*$^{-/-}$ microglia. The pathways downstream of mTOR are known to be involved in ribosomal activity, protein synthesis and energy generation through induction of HIF1α, glycolysis, and enhanced mitochondrial functioning (Hay and Sonenberg, 2004, Duvel et al., 2010). In fact, little is known on the role of mTOR in the diverse microglial phenotypes. *In vitro* experiments with primary microglia and BV2 cells showed increased mTOR signaling after exposure to hypoxia, LPS or a mixture of cytokines (Lu et al., 2006). Mouse models with various neurological conditions such as spinal cord injury and epilepsy, were shown to improve when treated with mTOR inhibitors but the impact on the inflammatory reaction remains poorly documented (Sekiguchi et al., 2012, van Vliet et

al., 2012, Lu et al., 2014). Interestingly, mTOR was recently identified as a novel factor involved in macrophage polarization although contradictory findings were reported whether mTOR activation biases the cytokine response towards a pro- or an anti-inflammatory state (Byles et al., 2013, Luo et al., 2014). In addition, it was recently shown that the AKT-mTOR-HIF1α pathway is instrumental for 'training' of macrophages whereby cytokine expression is enhanced following a prior exposure to β-glycan (Cheng et al., 2014, Saeed et al., 2014). This signaling orchestrates a switch in macrophages from oxidative metabolism to aerobic glycolysis. In this respect, the upregulation of the mTOR pathway in *Mfp2*$^{-/-}$ microglia, may play a broader role than only sustain growth and proliferation. The activation of the transcription factor HIF1α and its downstream glycolytic enzymes might play a pivotal role in the primed state of *Mfp2*$^{-/-}$ brain and possibly in other chronic neuroinflammatory states. In view of the premise that primed microglia in neurodegenerative diseases become detrimental after a systemic insult such as infection or illness, it is important to further investigate whether targeting mTOR can modify the microglia expression pattern in *Mfp2*$^{-/-}$ mice and in other neuroinflammatory conditions.

In conclusion, our data indicate that chronically reactive microglia in *Mfp2*$^{-/-}$ brain adopt an immunologically activated but non-polarized phenotype that is marked by morphological and metabolic adaptations. These microglia act in a pro-survival environment without overt neuronal demise, although an adverse effect on neuronal functioning through loss of microglial homeostatic functions cannot be excluded.

REFERENCES

Baes M, Huyghe S, Carmeliet P, Declercq PE, Collen D, Mannaerts GP, Van Veldhoven PP. 2000. Inactivation of the peroxisomal multifunctional protein-2 in mice impedes the degradation of not only 2-methyl branched fatty acids and bile acid intermediates but also of very long chain fatty acids. J Biol Chem 275:16329-16336.

Biber K, Owens T, Boddeke E. 2014. What is microglia neurotoxicity (Not)? Glia 62:841-854.

Block ML, Zecca L, Hong JS. 2007. Microglia-mediated neurotoxicity: uncovering the molecular mechanisms. Nat Rev Neurosci 8:57-69.

Bottelbergs A, Verheijden S, Hulshagen L, Gutmann DH, Goebbels S, Nave KA, Kassmann C, Baes M. 2010. Axonal integrity in the absence of functional peroxisomes from projection neurons and astrocytes. Glia 58:1532-1543.

Brown GC, Neher JJ. 2014. Microglial phagocytosis of live neurons. Nat Rev Neurosci 15:209-216.

Butovsky O, Jedrychowski MP, Moore CS, Cialic R, Lanser AJ, Gabriely G, Koeglsperger T, Dake B, Wu PM, Doykan CE, Fanek Z, Liu L, Chen Z, Rothstein JD, Ransohoff RM, Gygi SP, Antel JP, Weiner HL. 2014. Identification of a unique TGF-beta-dependent molecular and functional signature in microglia. Nat Neurosci 17:131-143.

Butovsky O, Siddiqui S, Gabriely G, Lanser AJ, Dake B, Murugaiyan G, Doykan CE, Wu PM, Gali RR, Iyer LK, Lawson R, Berry J, Krichevsky AM, Cudkowicz ME, Weiner HL. 2012. Modulating inflammatory monocytes with a unique microRNA gene signature ameliorates murine ALS. J Clin Invest 122:3063-3087.

Byles V, Covarrubias AJ, Ben-Sahra I, Lamming DW, Sabatini DM, Manning BD, Horng T. 2013. The TSC-mTOR pathway regulates macrophage polarization. Nat Commun 4:2834.

Cartier N, Aubourg P. 2010. Hematopoietic stem cell transplantation and hematopoietic stem cell gene therapy in X-linked adrenoleukodystrophy. Brain Pathology 20:857-862.

Cartier N, Hacein-Bey-Abina S, Bartholomae CC, Veres G, Schmidt M, Kutschera I, Vidaud M, Abel U, Dal-Cortivo L, Caccavelli L, Mahlaoui N, Kiermer V, Mittelstaedt D, Bellesme C, Lahlou N, Lefrere F, Blanche S, Audit M, Payen E, Leboulch P, l'Homme B, Bougneres P, Von KC, Fischer A, Cavazzana-Calvo M, Aubourg P. 2009. Hematopoietic stem cell gene therapy with a lentiviral vector in X-linked adrenoleukodystrophy. Science 326:818-823.

Cheng SC, Quintin J, Cramer RA, Shepardson KM, Saeed S, Kumar V, Giamarellos-Bourboulis EJ, Martens JH, Rao NA, Aghajanirefah A, Manjeri GR, Li Y, Ifrim DC, Arts RJ, van der Veer BM, Deen PM, Logie C, O'Neill LA, Willems P, van de Veerdonk FL, van der Meer JW, Ng A, Joosten LA, Wijmenga C, Stunnenberg HG, Xavier RJ, Netea MG. 2014. mTOR- and HIF-1alpha-mediated aerobic glycolysis as metabolic basis for trained immunity. Science 345:1250684.

Cherry JD, Olschowka JA, O'Banion MK. 2014. Neuroinflammation and M2 microglia: the good, the bad, and the inflamed. J Neuroinflammation 11:98.

Chiu IM, Morimoto ET, Goodarzi H, Liao JT, O'Keeffe S, Phatnani HP, Muratet M, Carroll MC, Levy S, Tavazoie S, Myers RM, Maniatis T. 2013. A neurodegeneration-specific gene-expression signature of acutely isolated microglia from an amyotrophic lateral sclerosis mouse model. Cell Rep 4:385-401.

De Haas AH, Boddeke HW, Brouwer N, Biber K. 2007. Optimized isolation enables ex vivo analysis of microglia from various central nervous system regions. Glia 55:1374-1384.

Derecki NC, Cronk JC, Kipnis J. 2013. The role of microglia in brain maintenance: implications for Rett syndrome. Trends Immunol 34:144-150.

Duvel K, Yecies JL, Menon S, Raman P, Lipovsky AI, Souza AL, Triantafellow E, Ma Q, Gorski R, Cleaver S, Vander Heiden MG, MacKeigan JP, Finan PM, Clish CB, Murphy LO, Manning BD. 2010. Activation of a metabolic gene regulatory network downstream of mTOR complex 1. Mol Cell 39:171-183.

Estevez AG, Sahawneh MA, Lange PS, Bae N, Egea M, Ratan RR. 2006. Arginase 1 regulation of nitric oxide production is key to survival of trophic factor-deprived motor neurons. J Neurosci 26:8512-8516.

584 Ferdinandusse S, Denis S, Mooyer PA, Dekker C, Duran M, Soorani-Lunsing RJ, Boltshauser E, Macaya
585 A, Gartner J, Majoie CB, Barth PG, Wanders RJ, Poll-The BT. 2006a. Clinical and biochemical
586 spectrum of D-bifunctional protein deficiency. Ann Neurol 59:92-104.
587 Ferdinandusse S, Denis S, Mooyer PAW, Dekker C, Duran M, Soorani-Lunsing RJ, Boltshauser E,
588 Macaya A, G„rtner J, Majoie CBLM, Barth PG, Wanders RJA, Poll-The BT. 2006b. Clinical and
589 biochemical spectrum of D-bifunctional protein deficiency. Ann Neurol 59:92-104.
590 Gautier EL, Shay T, Miller J, Greter M, Jakubzick C, Ivanov S, Helft J, Chow A, Elpek KG, Gordonov S,
591 Mazloom AR, Ma'ayan A, Chua WJ, Hansen TH, Turley SJ, Merad M, Randolph GJ. 2012.
592 Gene-expression profiles and transcriptional regulatory pathways that underlie the identity
593 and diversity of mouse tissue macrophages. Nat Immunol 13:1118-1128.
594 Giulietti A, Overbergh L, Valckx D, Decallonne B, Bouillon R, Mathieu C. 2001. An overview of real-
595 time quantitative PCR: applications to quantify cytokine gene expression. Methods 25:386-
596 401.
597 Glass CK, Saijo K, Winner B, Marchetto MC, Gage FH. 2010. Mechanisms underlying inflammation in
598 neurodegeneration. Cell 140:918-934.
599 Gomez-Nicola D, Fransen NL, Suzzi S, Perry VH. 2013. Regulation of microglial proliferation during
600 chronic neurodegeneration. J Neurosci 33:2481-2493.
601 Hay N, Sonenberg N. 2004. Upstream and downstream of mTOR. Genes Dev 18:1926-1945.
602 Hickman SE, Kingery ND, Ohsumi TK, Borowsky ML, Wang LC, Means TK, El Khoury J. 2013. The
603 microglial sensome revealed by direct RNA sequencing. Nat Neurosci 16:1896-1905.
604 Hochberg Y, Benjamini Y. 1990. More powerful procedures for multiple significance testing. Stat Med
605 9:811-818.
606 Hughes V. 2012. Microglia: The constant gardeners. Nature 485:570-572.
607 Hulshagen L, Krysko O, Bottelbergs A, Huyghe S, Klein R, Van Veldhoven PP, De Deyn PP, D'Hooge R,
608 Hartmann D, Baes M. 2008. Absence of functional peroxisomes from mouse CNS causes
609 dysmyelination and axon degeneration. J Neurosci 28:4015-4027.
610 Huyghe S, Mannaerts GP, Baes M, Van Veldhoven PP. 2006a. Peroxisomal multifunctional protein-2:
611 the enzyme, the patients and the knockout mouse model. BBA Mol Cell Biol L 1761:973-994.
612 Huyghe S, Schmalbruch H, De Gendt K, Verhoeven G, Guillou F, Van Veldhoven PP, Baes M. 2006b.
613 Peroxisomal multifunctional protein 2 is essential for lipid homeostasis in Sertoli cells and for
614 male fertility in mice. Endocrinology 147:2228-2236.
615 Huyghe S, Schmalbruch H, Hulshagen L, Van Veldhoven PP, Baes M, Hartmann D. 2006c. Peroxisomal
616 multifunctional protein-2 deficiency causes motor deficits and glial lesions in the adult CNS.
617 Am J Pathology 168:1321-1334.
618 Irizarry RA, Hobbs B, Collin F, Beazer-Barclay YD, Antonellis KJ, Scherf U, Speed TP. 2003. Exploration,
619 normalization, and summaries of high density oligonucleotide array probe level data.
620 Biostatistics 4:249-264.
621 Jia Y, Qi C, Zhang Z, Hashimoto T, Rao MS, Huyghe S, Suzuki Y, Van Veldhoven PP, Baes M, Reddy JK.
622 2003. Overexpression of peroxisome proliferator-activated receptor-alpha (PPARalpha)-
623 regulated genes in liver in the absence of peroxisome proliferation in mice deficient in both
624 L- and D- forms of enoyl-CoA hydratase/dehydrogenase enzymes of peroxisomal beta-
625 oxidation system. J Biol Chem 278:47232-47239.
626 Kemp S, Berger J, Aubourg P. 2012. X-linked adrenoleukodystrophy: metabolic, genetic and clinical
627 aspects. BBA-Mol Basis Dis 1822:1465-1474.
628 Khan A, Wei XC, Snyder FF, Mah JK, Waterham H, Wanders RJ. 2010. Neurodegeneration in D-
629 bifunctional protein deficiency: diagnostic clues and natural history using serial magnetic
630 resonance imaging. Neuroradiology 52:1163-1166.
631 Kigerl KA, Gensel JC, Ankeny DP, Alexander JK, Donnelly DJ, Popovich PG. 2009. Identification of two
632 distinct macrophage subsets with divergent effects causing either neurotoxicity or
633 regeneration in the injured mouse spinal cord. J Neurosci 29:13435-13444.
634 Lange PS, Langley B, Lu P, Ratan RR. 2004. Novel roles for arginase in cell survival, regeneration, and
635 translation in the central nervous system. J Nutr 134:2812S-2817S.

636 Liao B, Zhao W, Beers DR, Henkel JS, Appel SH. 2012. Transformation from a neuroprotective to a
637 neurotoxic microglial phenotype in a mouse model of ALS. Exp Neurol 237:147-152.
638 Lu DY, Liou HC, Tang CH, Fu WM. 2006. Hypoxia-induced iNOS expression in microglia is regulated by
639 the PI3-kinase/Akt/mTOR signaling pathway and activation of hypoxia inducible factor-
640 1alpha. Biochem Pharmacol 72:992-1000.
641 Lu Q, Gao L, Huang L, Ruan L, Yang J, Huang W, Li Z, Zhang Y, Jin K, Zhuge Q. 2014. Inhibition of
642 mammalian target of rapamycin improves neurobehavioral deficit and modulates immune
643 response after intracerebral hemorrhage in rat. J Neuroinflammation 11:44.
644 Luo L, Wall AA, Yeo JC, Condon ND, Norwood SJ, Schoenwaelder S, Chen KW, Jackson S, Jenkins BJ,
645 Hartland EL, Schroder K, Collins BM, Sweet MJ, Stow JL. 2014. Rab8a interacts directly with
646 PI3Kgamma to modulate TLR4-driven PI3K and mTOR signalling. Nat Commun 5:4407.
647 Norden DM, Godbout JP. 2013. Review: microglia of the aged brain: primed to be activated and
648 resistant to regulation. Neuropathol Appl Neurobiol 39:19-34.
649 Olah M, Raj D, Brouwer N, De Haas AH, Eggen BJ, Den Dunnen WF, Biber KP, Boddeke HW. 2012. An
650 optimized protocol for the acute isolation of human microglia from autopsy brain samples.
651 Glia 60:96-111.
652 Parkhurst CN, Yang G, Ninan I, Savas JN, Yates JR, 3rd, Lafaille JJ, Hempstead BL, Littman DR, Gan WB.
653 2013. Microglia promote learning-dependent synapse formation through brain-derived
654 neurotrophic factor. Cell 155:1596-1609.
655 Perry VH, Holmes C. 2014. Microglial priming in neurodegenerative disease. Nat Rev Neurol 10:217-
656 224.
657 Prinz M, Mildner A. 2011. Microglia in the CNS: immigrants from another world. Glia 59:177-187.
658 Prinz M, Priller J. 2014. Microglia and brain macrophages in the molecular age: from origin to
659 neuropsychiatric disease. Nat Rev Neurosci 15:300-312.
660 Ransohoff RM, Perry VH. 2009. Microglial physiology: unique stimuli, specialized responses. Annu
661 Rev Immunol 27:119-145.
662 Saeed S, Quintin J, Kerstens HH, Rao NA, Aghajanirefah A, Matarese F, Cheng SC, Ratter J, Berentsen
663 K, van der Ent MA, Sharifi N, Janssen-Megens EM, Ter Huurne M, Mandoli A, van Schaik T, Ng
664 A, Burden F, Downes K, Frontini M, Kumar V, Giamarellos-Bourboulis EJ, Ouwehand WH, van
665 der Meer JW, Joosten LA, Wijmenga C, Martens JH, Xavier RJ, Logie C, Netea MG,
666 Stunnenberg HG. 2014. Epigenetic programming of monocyte-to-macrophage differentiation
667 and trained innate immunity. Science 345:1251086.
668 Salter MW, Beggs S. 2014. Sublime microglia: expanding roles for the guardians of the CNS. Cell
669 158:15-24.
670 Sanagi T, Yuasa S, Nakamura Y, Suzuki E, Aoki M, Warita H, Itoyama Y, Uchino S, Kohsaka S, Ohsawa
671 K. 2010. Appearance of phagocytic microglia adjacent to motoneurons in spinal cord tissue
672 from a presymptomatic transgenic rat model of amyotrophic lateral sclerosis. J Neurosci Res
673 88:2736-2746.
674 Satoh J, Tabunoki H, Ishida T, Yagishita S, Jinnai K, Futamura N, Kobayashi M, Toyoshima I, Yoshioka
675 T, Enomoto K, Arai N, Arima K. 2011. Immunohistochemical characterization of microglia in
676 Nasu-Hakola disease brains. Neuropathology 31:363-375.
677 Sekiguchi A, Kanno H, Ozawa H, Yamaya S, Itoi E. 2012. Rapamycin promotes autophagy and reduces
678 neural tissue damage and locomotor impairment after spinal cord injury in mice. J
679 Neurotrauma 29:946-956.
680 Tremblay ME, Lowery RL, Majewska AK. 2010. Microglial interactions with synapses are modulated
681 by visual experience. PLoS Biol 8:e1000527.
682 van der Knaap MS, Wassmer E, Wolf NI, Ferreira P, Topcu M, Wanders RJ, Waterham HR,
683 Ferdinandusse S. 2012. MRI as diagnostic tool in early-onset peroxisomal disorders.
684 Neurology 78:1304-1308.
685 van Vliet EA, Forte G, Holtman L, den Burger JC, Sinjewel A, de Vries HE, Aronica E, Gorter JA. 2012.
686 Inhibition of mammalian target of rapamycin reduces epileptogenesis and blood-brain
687 barrier leakage but not microglia activation. Epilepsia 53:1254-1263.

688 Verheijden S, Bottelbergs A, Krysko O, Krysko DV, Beckers L, De Munter S, Van Veldhoven PP, Wyns S,
689 Kulik W, Nave KA, Ramer MS, Carmeliet P, Kassmann CM, Baes M. 2013. Peroxisomal
690 multifunctional protein-2 deficiency causes neuroinflammation and degeneration of Purkinje
691 cells independent of very long chain fatty acid accumulation. Neurobiol Dis 58:258-269.
692 Yamasaki R, Lu H, Butovsky O, Ohno N, Rietsch AM, Cialic R, Wu PM, Doykan CE, Lin J, Cotleur AC,
693 Kidd G, Zorlu MM, Sun N, Hu W, Liu L, Lee JC, Taylor SE, Uehlein L, Dixon D, Gu J, Floruta CM,
694 Zhu M, Charo IF, Weiner HL, Ransohoff RM. 2014. Differential roles of microglia and
695 monocytes in the inflamed central nervous system. J Exp Med 211:1533-1549.
696 Zhan Y, Paolicelli RC, Sforazzini F, Weinhard L, Bolasco G, Pagani F, Vyssotski AL, Bifone A, Gozzi A,
697 Ragozzino D, Gross CT. 2014. Deficient neuron-microglia signaling results in impaired
698 functional brain connectivity and social behavior. Nat Neurosci 17:400-406.

699

700

701

702

703

704 **ACKNOWLEDGMENTS**

705 The authors wish to thank Benno Das and Lies Pauwels for excellent technical assistance, Nieske
706 Brouwer and Prof. dr. H.W.G.M. Boddeke (Rijksuniversiteit Groningen, The Netherlands) for the
707 guidance with the microglia isolation and Prof L. Van Den Bosch (VIB and KU Leuven, Belgium) for
708 providing sections of spinal cord of *SOD1*^{G93A} mice. This work was funded by grants from Fonds
709 Wetenschappelijk Onderzoek Vlaanderen (G.0675.12N and G.0A15.13), and KU Leuven (OT12/79).

FIGURE LEGENDS

Figure 1. Increased numbers of myeloid cells in *Mfp2*$^{-/-}$ brain do not derive from influx of peripheral monocytes but from proliferation of resident microglia

(A) Immunofluorescent staining for the microglia/macrophage marker Iba-1 reveals an increased number and altered shape of brain myeloid cells in the CA3 region of hippocampus in *Mfp2*$^{-/-}$ mice at 5 months compared to an age-matched control. Quantification of Iba-1^{+} cells in different brain regions shows increased microglia cell numbers in hippocampus (hpc), motor cortex (mcor) and pons of *Mfp2*$^{-/-}$ mice (** $p < 0.01$). Nuclei are stained blue with DAPI. (B) FACS analysis of Ly6C expression in CD11b-gated cells (n = 6 per group). Quantification shows that nearly all CD11b^{+} cells in brain of control and *Mfp2*$^{-/-}$ mice are Ly6c negative. (C) Nearly all Cd11b^{+} myeloid cells from control and *Mfp2*$^{-/-}$ brain express the microglial specific surface marker CD39 (n = 6 per group). (D) Nearly all Cd11b^{+} myeloid cells from control and *Mfp2*$^{-/-}$ brain express the microglial specific surface marker FCRLS (n = 4 per group). All FACS data are presented as mean ± SEM (n = 4- 6 per group) **$p < 0.01$. (E) BrdU incorporation (green) in Iba-1^{+} cells (red) in *Mfp2*$^{-/-}$ but not in control brain using immunofluorescent staining. Nuclei are stained blue with DAPI. (F,G) BrDU incorporation in CD11b-gated cells is higher in *Mfp2*$^{-/-}$ compared to control mice (n = 3-4 per group, mean ± SEM) *$p < 0.05$.

Figure 2. Abundant microglia-neuron contacts but no neuronal loss in *Mfp2*$^{-/-}$ mice

(A-D) Activated microglia (Iba1^{+}, green) enwrap cell bodies (DAPI, blue) in the CA3 region of the hippocampus in *Mfp2*$^{-/-}$ mice (C,D) but not in control (A,B). B and D are magnifications of the highlighted area in A and C, respectively. Nuclei are stained blue with DAPI. (E) F4/80^{+} cells contact NeuN^{+} neurons in the brainstem of *Mfp2*$^{-/-}$ mice. (F) Magnification of E. (G – I) H&E staining and quantification in the CA3 region of hippocampus reveals preservation of neurons in *Mfp2*$^{-/-}$ mice.

Figure 3. Transcriptomics analysis on acutely isolated microglia from control and *Mfp2*$^{-/-}$ mouse brain

(A,B) Cd11b/Cd45 FACS sorting of microglia isolated from control (A) and *Mfp2*$^{-/-}$ (B) mouse brain. (C) Volcano plot of differentially expressed genes of *Mfp2*$^{-/-}$ versus control microglia (cut-off: 0.75 ≥ fold change ≥ 1.5; $p < 0.01$). (D) The 10 most upregulated pathways after applying the canonical pathway enrichment tool of Ingenuity software on the microarray dataset of *Mfp2*$^{-/-}$ microglia (differentially expressed genes: 0.75 ≤ fold ≤1.5; p-value 0.01). (E,F) Increased IHC staining for phosphorylated ribosomal S6 (pS6, green), a downstream target of mTOR, in Iba1^{+} microglia (red) in *Mfp2*$^{-/-}$ mice (F) as compared to control (E), shown for thalamus region.

Figure 4. Differences in expression of lysosomal, phagocytic and nitrosative stress markers in *Mfp2*$^{-/-}$ versus *SOD1*^{G93A} microglia

(A-B) After transcriptomics analyses of *Mfp2*$^{-/-}$ microglia (A) and *SOD1*^{G93A} microglia (B) (data from GEO GSE43366) the expression of genes associated with the Lysosome (*mmu04142*) KEGG pathway were plotted. The percentage of genes of this pathway differentially expressed in both mouse models is shown. (C) Heatmap for enriched functions of *SOD1*^{G93A} microglia as compared to *Mfp2*$^{-/-}$ microglia (Ingenuity analysis). Enrichment is depicted as activated (orange), not enriched (white) or deactivated (blue). Red arrows point to functions related to phagocytosis, green arrows to growth and proliferation. (D-F) Staining of the lysosomal marker Cathepsin D (green) in visual cortex of control (D) and *Mfp2*$^{-/-}$ mice (E) and in spinal cord of endstage SOD1^{G93A} mice (F). (G-I) Co-staining of the microglial marker Iba1 (red) and the lysosomal marker LAMP2/MAC3 (green) in brainstem of control (G) and *Mfp2*$^{-/-}$ mice (H) and in spinal cord of endstage SOD1^{G93A} mice (I). White arrowheads point to LAMP2^{+} microglia. (J-L) Staining for nitrosylated proteins (green) in visual cortex of control (J) and *Mfp2*$^{-/-}$ mice (K) and in spinal cord of endstage SOD1^{G93A} mice (L). Nuclei are stained blue with DAPI.

Figure 5. The immunological profile of *Mfp2*$^{-/-}$ microglia is not polarized to a pro- or anti-inflammatory state

(A) Relative transcript levels of pro-inflammatory (dark gray bars) and anti-inflammatory (white bars) activation markers as determined by microarray analysis in *Mfp2*$^{-/-}$ microglia compared to wild type (n=4). (B) qRT-PCR analyses of the pro-inflammatory markers IL1β and IL6 and the anti-inflammatory

764 marker Arg-1 confirm micro-array data and indicate that microglia are not unequivocally polarized.
765 mRNA expression levels were normalized to β-actin. Data are presented as mean ± SEM (n = 3-4). * p
766 < 0.05; ** p < 0.01. (C) Surface markers expression associated with classical (gray) and alternative
767 (white) macrophage activation as determined by microarray analysis. (D) FACS analysis of $CD11b^{+}$
768 microglia shows increased expression of CD11c and F4/80 surface markers associated with classical
769 activation. There is also increased expression of the anti-inflammatory marker $CD204^{pos}$ (Msr1) as
770 well as an increase in the proportion of microglia that are $CD206^{neg}$ (Mrc1) (representative experiment
771 out of two). (E-F) *Mfp2*$^{-/-}$ and control mice (n=3-5) were challenged with intraperitoneal LPS and
772 brainstem tissue was analyzed after 4 hrs. Transcripts (E) and cytokine levels (F) of *Il1b, Il6* and *Tnf*
773 were more elevated in *Mfp2*$^{-/-}$ as compared to control mice. # = not detectable, * p<0.05, ** p < 0.01,
774 ***p<0.001.
775
776 **Figure 6. Repression of homeostatic gene signature in *Mfp2*$^{-/-}$ microglia**
777 (A) Heatmap showing expression values of signature genes of microglia (according to Butovsky et al,
778 2013) in control versus *Mfp2*$^{-/-}$ microglia. In *Mfp2*$^{-/-}$ microglia, 40 out of 86 genes are significantly
779 downregulated (47%). Expression values are expressed as robust multi-array analysis (RMA). (B,C)
780 qRT-PCR confirms the downregulation of the microglia-enriched genes *Cx3cr1* (A) and *Tgfbr1* (B) in
781 *Mfp2*$^{-/-}$ microglia. Expression levels were normalized to β-actin. Data are presented as mean ± SEM (n
782 = 3-4, ** p < 0.01; *** p < 0.001). (D,E) Immunohistochemical staining confirms downregulation of the
783 purinergic receptor P2RY12 on microglia of *Mfp2*$^{-/-}$ as compared to wild type mice. (F,G) FACS
784 analysis of $CD11b^{+}$ microglia shows reduced expression of CX3CR1 and to a lesser extent of IL10R
785 in *Mfp2*$^{-/-}$ microglia (1 experiment out of 2 with similar data).
786
787 **Supplemental figure 1 Transcriptomics analysis of isolated microglia from *Mfp2*$^{-/-}$ and control**
788 **brain**
789 (A) Heatmap and unsupervised hierarchical clustering of RMA values. (B) Principle component
790 analysis (PCA) of gene expression data. (C) Heatmaps of top 50 genes upregulated and
791 downregulated in *Mfp2*$^{-/-}$ as compared to wild type microglia, ranked by fold change.
792

793

Figure 1

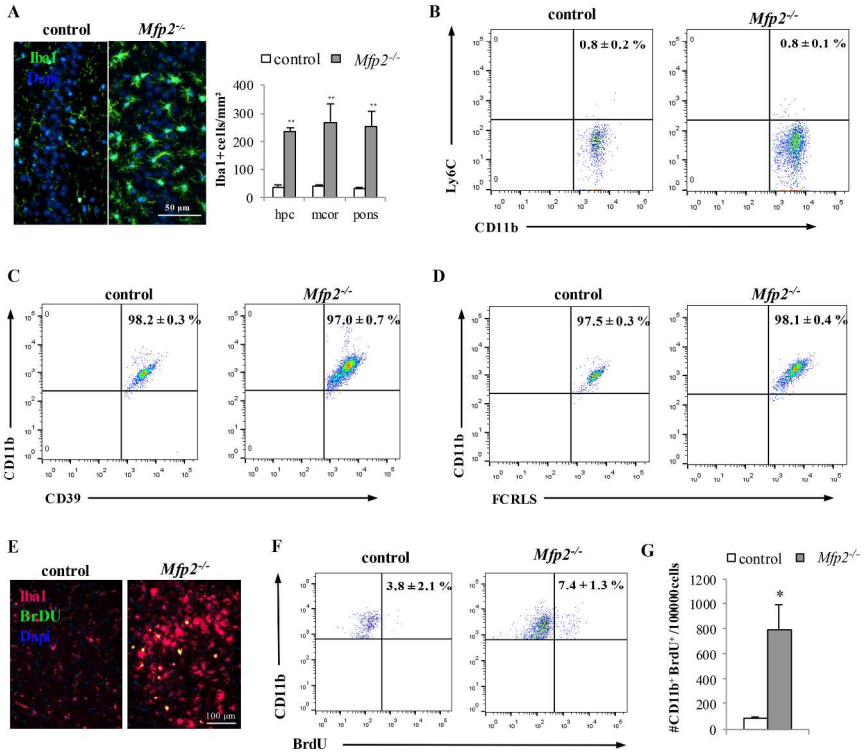

Figure 1

Figure 2

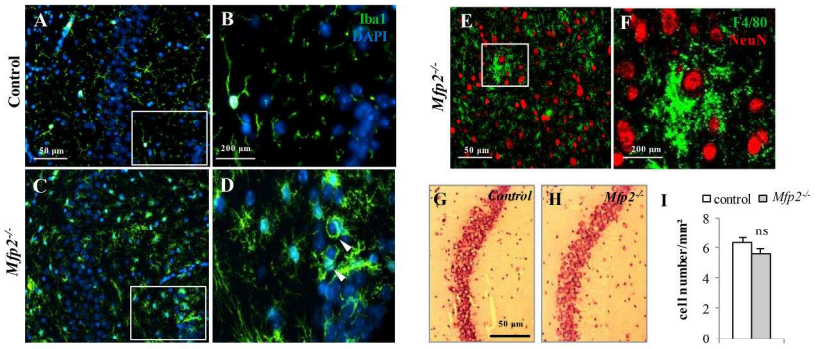
A
B
Iba1
DAPI
Control
50 µm
200 µm
C
D
Mfp2-/-
E
F
F4/80
NeuN
Mfp2-/-
50 µm
200 µm
G
Control
H
Mfp2-/-
50 µm
I
control
Mfp2-/-
ns
cell number/mm²
8
6
4
2
0

Figure 3

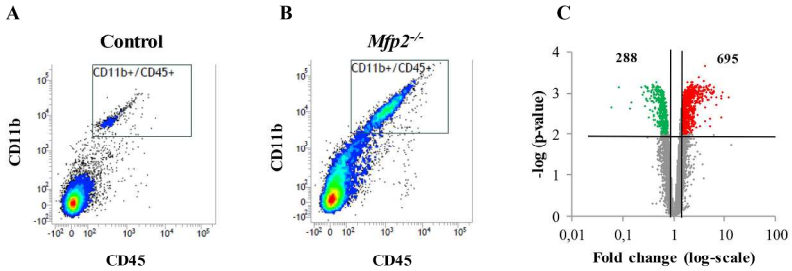

D

Canonical pathway	p-value of enrichment
EIF2 Signaling	5.01E-49
mTOR Signaling	2.51E-18
Regulation of eIF4 and p70S6K Signaling	7.94E-15
Glycolysis I	1.91E-07
Mitochondrial Dysfunction	4.90E-05
IL-8 Signaling	1.20E-04
Ephrin B Signaling	2.75E-04
LXR/RXR Activation	3.02E-04
TREM1 Signaling	3.16E-04
Gluconeogenesis I	3.98E-04

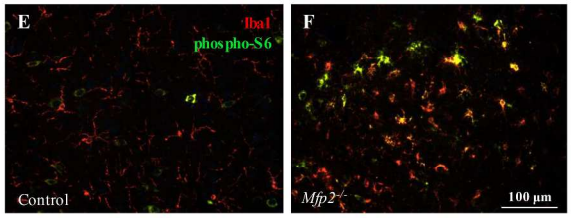

Figure 3

Figure 4

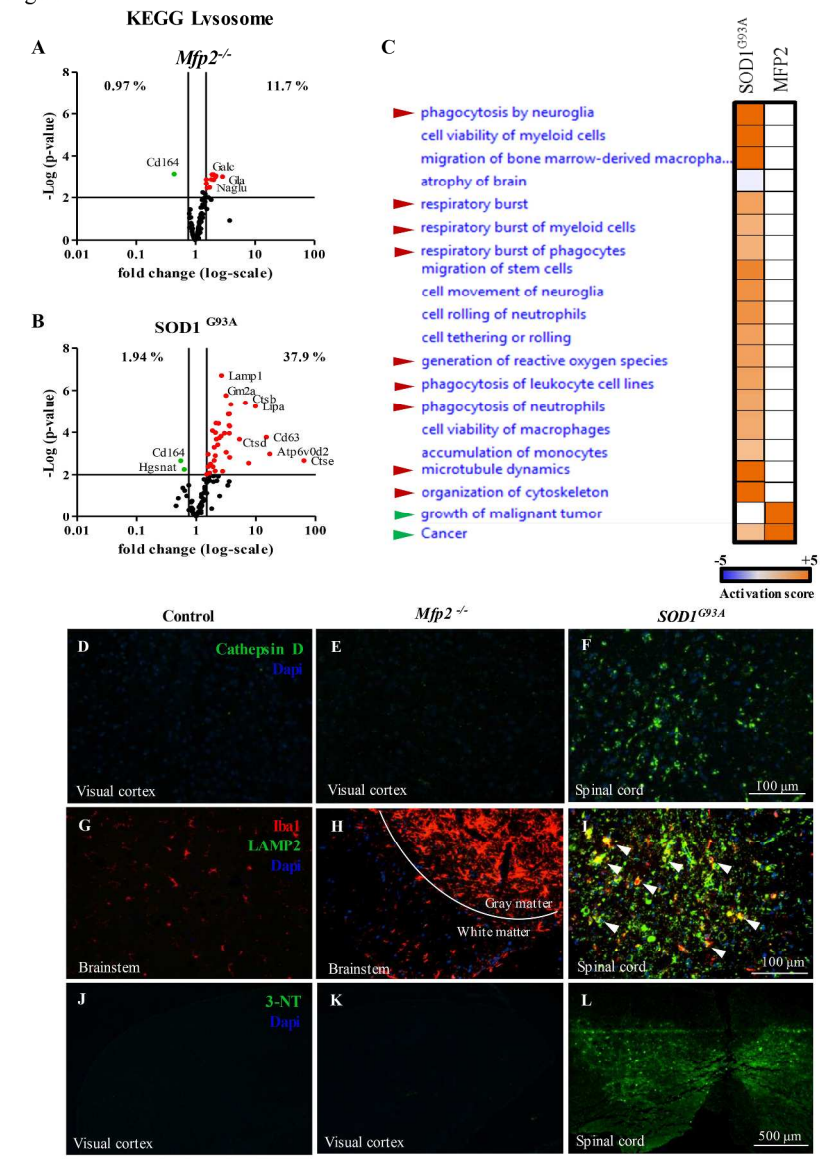

Figure 4

Figure 5

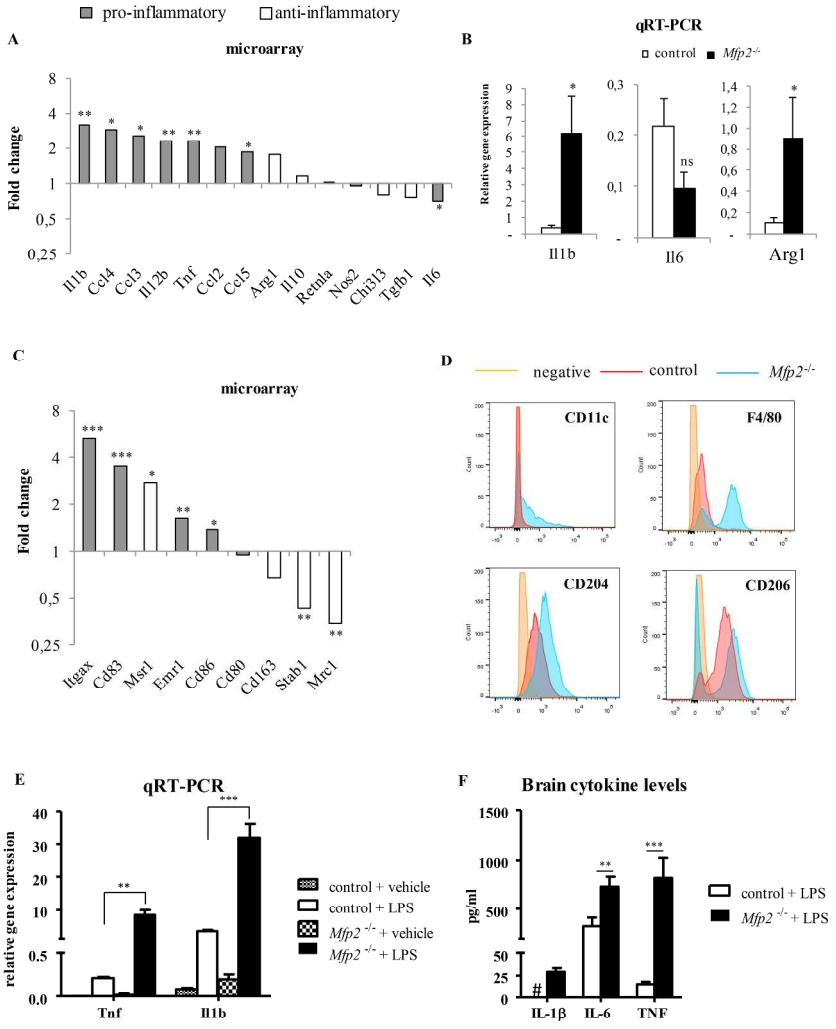

Figure 5

Figure 6

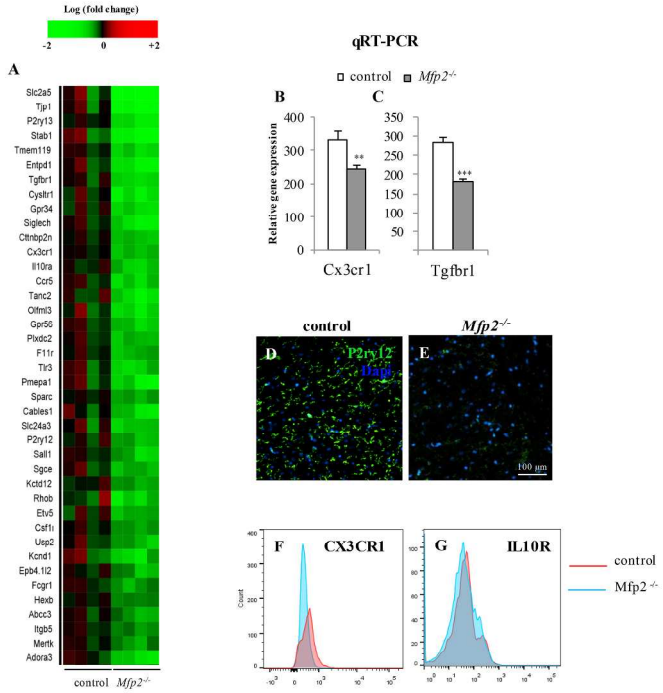

Figure 6

Supplemental Table 1: Altered gene expression in *Mfp2*$^{-/-}$ microglia according to micro-array analysis

Symbol	Name	Fold change
INFLAMMATION		
Chemokines and Cytokines		
Ccl2	chemokine (C-C motif) ligand 2	2.04
Ccl3	chemokine (C-C motif) ligand 3	2.55*
Ccl4	chemokine (C-C motif) ligand 4	2.91*
Ccl5	chemokine (C-C motif) ligand 5	1.87*
Ccl12	chemokine (C-C motif) ligand 12	2.76**
Ccl24	chemokine (C-C motif) ligand 24	0.51***
Cxcl10	chemokine (C-X-C motif) ligand 10	2.16*
Cxcl13	chemokine (C-X-C motif) ligand 13	12.97*
Cxcl16	chemokine (C-X-C motif) ligand 16	2.50***
Spp1	secreted phosphoprotein 1	8.25**
Il1b	interleukin 1 beta	3.23**
Il12b	interleukin 12b	2.33**
Tnf	tumor necrosis factor	2.32*
Il6	interleukin 6	0.70*
Toll-like receptors		
Tlr2	toll-like receptor 2	1.74**
Tlr3	toll-like receptor 3	0.65**
Tlr4	toll-like receptor 4	0.70**
Antigen presenting cell markers		
Itgax	integrin alpha X	5.28***
Nrp1	neuropilin 1	3.77***
Cd83	CD83 antigen	3.55***
Cd86	CD86 antigen	1.37*
Cd80	CD80 antigen	0.94
Neurotoxicity		
Nos2	nitric oxide synthase 2, inducible	0.94
Cybb	cytochrome b-245, beta polypeptide	1.61
Cyba	cytochrome b-245, alpha polypeptide	1.45*
Ncf4	neutrophil cytosolic factor 4	1.12
Ncf1	neutrophil cytosolic factor 1	0.94
CELL SURVIVAL		
Cell death		
Abl1	C-abl oncogene 1, non-receptor tyrosine kinase	0.63*
Anxa5	Annexin A5	2.86**
Atf5	Activating transcription factor 5	1.79**
Bag1	Bcl2-associated athanogene 1	1.44*
Bax	Bcl2-associated X protein	1.48**
Bcl2	B-cell leukemia/lymphoma 2	1.35*

Bnip3	BCL2/adenovirus E1B interacting protein 3	2.14**
Casp12	Caspase 12	0.69
Casp3	Caspase 3	0.67*
Casp4	Caspase 4, apoptosis-related cysteine peptidase	1.44*
Casp8	Caspase 8	0.62**
Proliferation		
Ccnb2	Cyclin B2	1.61
Ccnd1	Cyclin D1	0.51**
Ccnd2	Cyclin D2	1.44*
Cdkn1a	Cyclin-dependent kinase inhibitor 1A (P21)	1.66*
Cks1b	CDC28 protein kinase 1b	2.19**
Rad21	RAD21 homolog (S. pombe)	0.81*
Csf1	colony stimulating factor 1 (macrophage)	3.99***
Csf1r	colony stimulating factor 1 receptor	0.78*
Igf1	insulin-like growth factor 1	2.38**
Igf1r	insulin-like growth factor I receptor	0.73
Cd34	CD34 antigen	3.48**
Lgals3	lectin, galactose binding, soluble 3	2.01**
METABOLISM		
mTOR signaling		
Rps6	Ribosomal protein S6	2.84***
Rpsa	ribosomal protein SA	2.72***
Rps19	ribosomal protein S19	2.46***
Prr5l	proline rich 5 like	2.39**
Igf1	Insulin-like growth factor 1	2.38**
Rps18	ribosomal protein S18	2.30***
Rps26	ribosomal protein S26	2.22***
Rragd	Ras-related GTP binding D	2.19**
Rps5	ribosomal protein S5	2.19***
Fau	Finkel-Biskis-Reilly murine sarcoma virus (FBR-MuSV) ubiquitously expressed	2.17***
Pld3	phospholipase D family. member 3	2.09***
Hif1a	Hypoxia inducible factor 1, alpha subunit	2.06***
Eif3f	eukaryotic translation initiation factor 3. subunit F	2.01***
Rps2	ribosomal protein S2	1.95**
Rps25	ribosomal protein S25	1.92**
Rps12	ribosomal protein S12	1.91**
Rps16	ribosomal protein S16	1.90**
Rps23	ribosomal protein S23	1.89**
Rps11	ribosomal protein S11	1.82**
Rps13	ribosomal protein S13	1.82**
Vegfa	Vascular endothelial growth factor A	1.82**
Rps9	ribosomal protein S9	1.81***
Rps7	ribosomal protein S7	1.80**
Rps15	ribosomal protein S15	1.78***

Rps24	ribosomal protein S24	1.77**
Eif3h	eukaryotic translation initiation factor 3. subunit H	1.76**
Rps27l	ribosomal protein S27L	1.73**
Eif3k	eukaryotic translation initiation factor 3. subunit K	1.68**
Rps8	ribosomal protein S8	1.66**
Eif4ebp1	Eukaryotic translation initiation factor 4E binding protein 1	1.63**
Rps14	ribosomal protein S14	1.62**
Rps21	ribosomal protein S21	1.62**
Eif3e	eukaryotic translation initiation factor 3. subunit E	1.59**
Dgkz	Diacylglycerol kinase, zeta	1.58**
Rps4x	ribosomal protein S4X	1.55**
Rps3	ribosomal protein S3	1.55**
Rps27	ribosomal protein S27	1.53**
Eif4b	Eukaryotic translation initiation factor 4B	1.53**
Eif4b	eukaryotic translation initiation factor 4B	1.53**
Prkaa2	Protein kinase, AMP-activated, alpha 2 catalytic subunit	1.39*
Rragc	Ras-related GTP binding C	1.35*
Vegfb	Vascular endothelial growth factor B	1.27*
Rps6ka2	Ribosomal protein S6 kinase, polypeptide 2	1.62**
Pik3ca	Phosphatidylinositol 3-kinase, catalytic, alpha polypeptide	0.78*
Akt3	Thymoma viral proto-oncogene 3	0.75*
Pik3cg	Phosphoinositide-3-kinase, catalytic, gamma polypeptide	0.74**
Rps6ka1	Ribosomal protein S6 kinase polypeptide 1	0.70**
Rps6ka5	Ribosomal protein S6 kinase, polypeptide 5	0.70*
Sgk1	Serum/glucocorticoid regulated kinase 1	0.66*
Pten	Phosphatase and tensin homolog	0.66*
Ppml1	protein phosphatase. Mg2+/Mn2+ dependent. 1L	0.57**
Pld1	Phospholipase D1	0.54**
Prkab1	Protein kinase, AMP-activated, beta 1 non-catalytic subunit	0.53**
Prkca	Protein kinase C, alpha	0.43**
Prkcq	protein kinase C. theta	0.36***
Glycolysis		
Aldoa	aldolase A, fructose-bisphosphate	1.98***
Eno1	enolase 1, (alpha)	1.86**
Gapdh	glyceraldehyde 3-phopshate dehydrogenase	1.66**
Gpi	glucose-6-phosphate isomerase	1.86**
Pfkl	phosphofructokinase, liver	1.83***
Pgam1	phosphoglycerate mutase 1 (brain)	2.17**
Pgk1	phosphoglycerate kinase 1	2.10***
Pkm	pyruvate kinase, muscle	1.81***
Tpi1	triosephosphate isomerase 1	2.05***
Mitochondria		
Atp5d	ATP synthase. H+ transporting. mitochondrial F1 complex. delta subunit	1.59**
Atp5g2	ATP synthase. H+ transporting. mitochondrial Fo complex. subunit	1.65**

	C2 (subunit 9)	
Cox4I1	cytochrome c oxidase subunit IV isoform 1	1.89***
Cox6a1	cytochrome c oxidase subunit VIa polypeptide 1	1.54*
Cox6a2	cytochrome c oxidase subunit VIa polypeptide 2	8.86***
Cox6b1	cytochrome c oxidase subunit VIb polypeptide 1 (ubiquitous)	1.51**
Cox6c	cytochrome c oxidase subunit VIc	1.68**
Cox7a2l	cytochrome c oxidase subunit VIIa polypeptide 2 like	1.74**
Cox8a	cytochrome c oxidase subunit VIIIA (ubiquitous)	1.89**
Fis1	fission 1 (mitochondrial outer membrane) homolog (S. cerevisiae)	1.55**
Ndufa1	NADH dehydrogenase (ubiquinone) 1 alpha subcomplex. 1. 7.5kDa	2.13**
Ndufa2	NADH dehydrogenase (ubiquinone) 1 alpha subcomplex. 2. 8kDa	1.61**
Nudfb9	NADH dehydrogenase (ubiquinone) 1 beta subcomplex. 9. 22kDa	1.59**
Psen2	presenilin 2	1.61**
Uqcr11	ubiquinol-cytochrome c reductase. complex III subunit XI	2.18**
Uqcrh	ubiquinol-cytochrome c reductase. Complex III subunit VI	1.96***
Xdh	xanthine dehydrogenase	4.41***

The fold change in expression in *Mfp2*$^{-/-}$ microglia versus control is listed. *p<0.05; **p<0.01, ***p<0.001

Supplementary figure 1

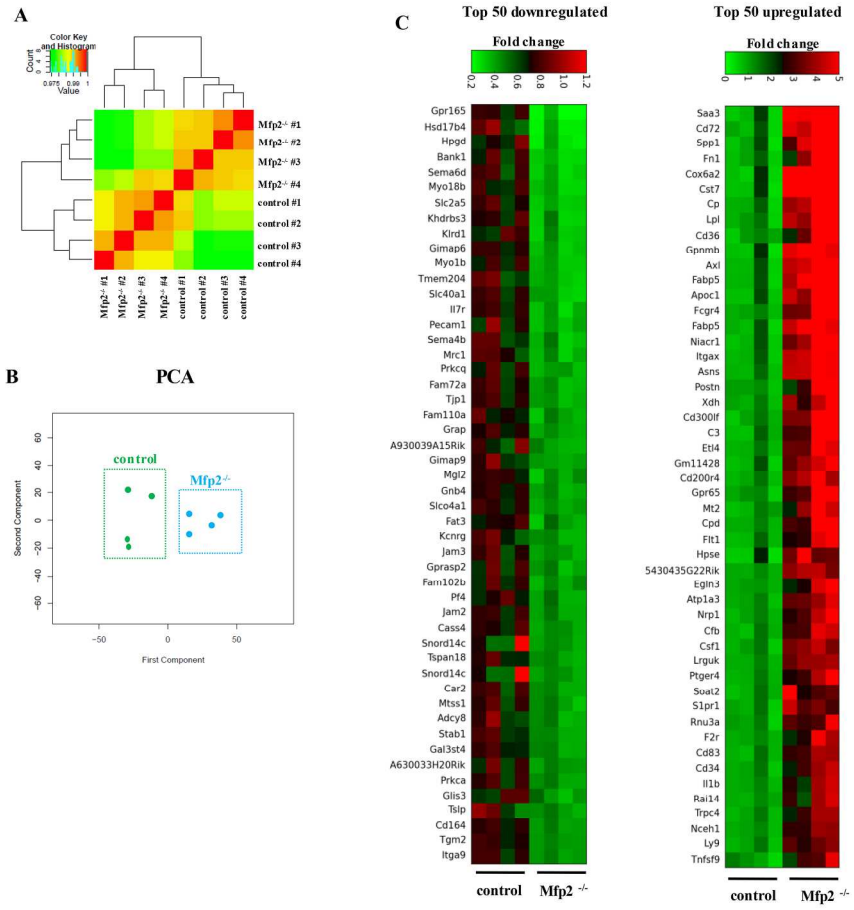

Supplementary figure 1